JOURNAL OF OPTOELECTRONICS AND ADVANCED MATERIALS Vol. 10, No. 1, January 2008, p. 104 - 109

Magnetoresistance sensors with magnetic layers for high sensitivity measurements

M. VOLMER*, J. NEAMTU[a], M. AVRAM[b]
Physics Department, Transilvania University, 29 Eroilor, Brasov 500036, Romania
[a]*Advanced Research Institute for Electrical Engineering, Splaiul Unirii 313, Bucharest, 030138, Romania*
[b]*National Institute for Research and Development in Microtechnologies, Str. Erou Iancu Nicolae 32B, 72996 Bucharest, Romania*

In this study we present an overview of the sensors made from magnetic layers and nanostructured systems. Fundamental and technological aspects are presented. A review of the spin valve mechanism is presented. A spin valve device consists of two ferromagnetic layers, separated by a Cu spacer. When the Cu layer is replaced by a thin insulator layer (Al_2O_3) then, we have a magnetic tunnel junction or, for some deposition conditions, a nanogranular system. Electrical and magnetic characterization of the magnetic layers and nanogranular systems plays an important role in the designing process of these sensors and some results are presented in this paper. For a better understanding of the magnetization processes that take place in these systems, micromagnetic simulations were performed as well. Finally, we present a method to increase the response quality of a rotation sensor based on the anisotropic magnetoresistance effect and a detection system of the magnetic particles employed in biology as markers or as carriers for targeted drug delivery.

(Received September 25, 2007; accepted January 10, 2008)

Keywords: Thin films, Magnetoresistance effect, Magnetic sensors, Micromagnetic simulation

1. Theoretical aspects

Magnetoresistance effect (MR) which arises in Permalloy based thin films is an attractive solution for the fabrication of magnetic sensors. The resistance behaviour of such thin films (3*d* ferromagnetic alloys) is anisotropic with respect to the applied field direction, the MR being positive when the magnetic field is parallel to the current (longitudinal) and negative when the magnetic field is perpendicular to the current direction (transversal). This is the anisotropic magnetoresistance effect (AMR) and it was discovered in 1857 by William Thomson (Lord Kelvin). The AMR effect arises from anisotropic scattering due to spin orbit-orbit interaction. It is worth to mention that the MR effect in ferromagnetic thin films is determined by the sample magnetization rather than the external magnetic field, *H*. The resistance produced by scattering is maximum when the magnetization direction is parallel (i.e. 0º or 180º) to the current direction and minimum when the magnetization is perpendicular to the current.

In general, the resistance is given as a function of the angle, θ, between the magnetization and current:

$$R = R_0 + \Delta R_{AMR} \cos^2 \theta \qquad (1)$$

Here, $\Delta R_{AMR}=R_l-R_t$ is the amplitude of the AMR effect calculated in the saturated state when the applied magnetic field is parallel and perpendicular to the current respectively. Usually, R_0 is the resistance in the saturated state when *H* is applied perpendicular to the current direction but in the film plane. The magnetoresistance ratio $\Delta R_{AMR}/R_0$ is relatively large for ternary Fe-Co-Ni alloys containing 70 to 90 atomic percent of Ni, amounting to at most 2.5 to 3 % in 30 nm Permalloy ($Ni_{81}Fe_{19}$) films [1]. This is because when the film thickness becomes comparable or smaller than the mean free path of the carriers we should take in account the scattering processes at the surfaces and interfaces which lower the amplitude of the MR effects. For many applications in read heads and other sensors, Permalloy (Py) is the preferred choice due to its favourable soft magnetic properties. In the ternary Fe-Co-Ni diagram the Permalloy composition lies close to both to zero magnetostriction and the zero crystalline anisotropy line. Therefore, the magnetic behaviour of the prepared Permalloy films is dominated by the uniaxial in-plane anisotropy induced by a field applied during deposition. Thus, for a field along the hard axis, i.e. perpendicular to the anisotropy direction, the change of the magnetisation will result from a coherent magnetization rotation process.

The plot of eq. 1 shows that the maximum sensitivity and linearity is achieved when the magnetization is at 45º with respect to the current. The 45º alignment is commonly achieved by patterning diagonal stripes of highly conductive metal (gold) onto the more resistive AMR material as shown in Fig. 1a. The current will then run perpendicular to these “barber pole” stripes while the magnetization vector remains preferentially along the long direction of the MR device. The application of an external magnetic field will rotate the magnetization with a resulting change in resistance as shown in Fig 1b. The MR ratio for AMR materials is typically a few percent.

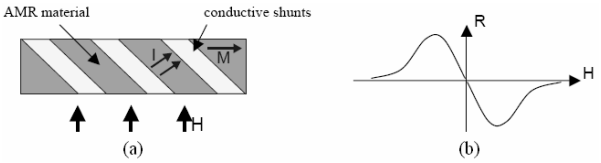

Fig. 1. (a) Barber-pole structure of conductive shunts that constrain the current to run at 45° to the rest position for the magnetization. (b) Resistance versus field for a properly biased AMR device.

To develop practical applications, such as contactless potentiometer or magnetic field sensors, it must to minimize the thermal drift and to optimize the MR response. For this purpose it is convenient to operate the device with the two or four active arms of a Wheatstone bridge. Each arm corresponds to one MR element. We have to mention here that many other materials can be used for this application. Granular manganese perovskites, having ferromagnetic transitions above room temperature, are good candidates for use as magnetoresistive sensors [2]. Using thick films of $La_{2/3}Sr_{1/3}MnO_3$ prepared by screen printing on polycrystalline Al_2O_3 it can be developed a room temperature AMR sensor to build a contactless potentiometer.

Because of the AMR effect will appear an electric field perpendicular to the applied current, in a Hall effect geometry, even when the magnetic field is in the film plane but it makes an angle θ=45° with the current direction [3, 4]. This is the so-called planar Hall effect (PHE). In Fig. 2 we present the field dependence of the PHE effect measured in a nanogranular Py(2nm)/Al_2O_3(1 nm)Py(2 nm) thin film [5].

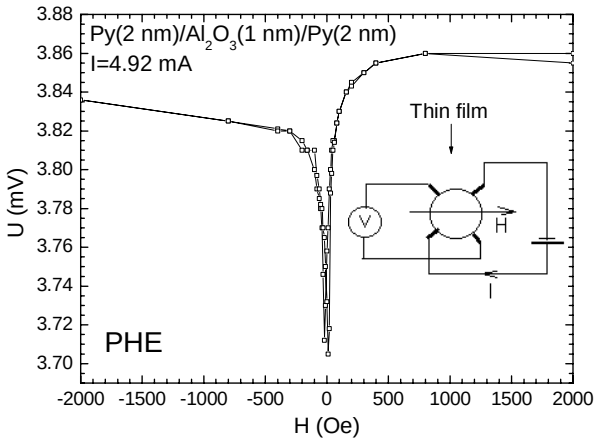

Fig. 2. Field dependence of the PHE for Py/AlO/Py thin film near the percolation limit. In inset is presented the experimental setup.

In this way we get direct access to the anisotropic part of the resistance with the advantage of a reduced thermal drift of the output signal. The sensitivity is about 0.04 mV/Oe for a magnetic field variation less 200 Oe and can be increased by a careful choice of the layers thickness, increasing the precision of the measuring setup, using high current pulses, etc. This plot suggests the main utility of the PHE, for building high sensitivity magnetic field sensors.

In a single domain approximation, the PHE voltage is determined by the relation [4, 6]:

$$U = CM^2 j \sin 2\theta \equiv A \sin 2\theta \qquad (2)$$

where C is a constant determined by the material properties, j is the current density, M is the saturation magnetization and θ is the angle between the current and the magnetization vector that, in turn, is determined by the value and direction of the external magnetic field.

From eq.2, we see how the PHE effect can provide information about the magnetic properties of the material and allows building of low-cost rotation sensors.

The giant magnetoresistance (GMR) effect in thin-film multilayers was discovered in 1988 by Baibich and coworkers at the Université Paris-Sud on a Fe/Cr multilayer structure. The term giant magnetoresistance was coined because the 10-15% change in resistance found in GMR far exceeds that of any AMR devices. A GMR device consists of two or more layers of ferromagnetic metal (typically NiFe, CoFe or related transition metal alloy) separated by ultra-thin non-magnetic metal spacer layers (Cu, Au or Ru), Fig. 3.

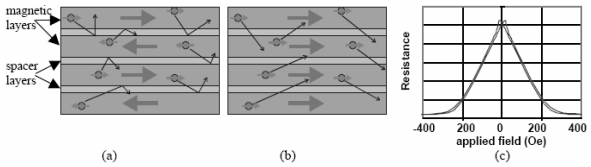

Fig. 3. Illustration of the GMR effect with (a) layers of alternating magnetization producing lots of scattering and (b) reduced scattering when the magnetization of the layers is aligned by an applied field. (c) Variation in resistance as a function of the applied field.

To obtain the GMR effect, the spacer layers must be thin compared to the mean free path of electrons so that electrons spin polarized in one layer can pass into the other layers before their polarization is disturbed by scattering. Essentially, one can think of the ferromagnetic layers as polarizing filters for the spin of the electrons. The spacer layers allow the magnetic directions of the layers to differ while still permitting the passage of electrons. When the magnetic layers are aligned in the same direction, electrons originating in one layer may pass relatively freely through the other layers as illustrated in Fig. 3a. However, if the magnetizations are opposing, then electrons originating in one layer are blocked from the adjacent layer (Fig. 3b). The disruption of the free motion of the electrons results in an increase in the electrical resistance [1]. This is the so called spin dependent scattering mechanism and the devices which are using this phenomenon are named "spin-valve" devices. If we consider the most common case of two ferromagnetic layers separated by a non magnetic layer, than the

resistance dependence on the angle θ between the magnetization directions from these two layers is expressed by [1]:

$$R = R_0 + \frac{\Delta R_{GMR}}{2}\left(1 - \cos\theta\right) \tag{3}$$

where R_0 is the structure resistance at the saturated state and ΔR_{GMR} is the amplitude of the GMR effect.

Basically there are two methods to obtain the antiparallel orientation of the magnetizations in the adjacent layers and hence the GMR effect: (i) the nonmagnetic layer has such a thickness (about 1 nm) for which the coupling between the adjacent ferromagnetic layers is an antiferromagnetic one and (ii) the magnetization of a ferromagnetic layer is pinned through exchange biasing effect using an antiferromagnetic layer of FeMn. So only the magnetization from the second layer known also as sensing layer is free to rotate. From technological point of view, the second method is the most applicable one and offers a high sensitivity at low magnetic fields. A typical "exchange-biased spin-valve" structure is [1] Si/SiO_2/Ta(3 nm)/Py(8 nm)/Cu(2.5 nm)/Py(6 nm)/$Fe_{50}Mn_{50}$(8 nm)/Ta(3 nm).

A typical magnetization curve and field dependence of an exchange-biased spin valve are presented in Fig. 5. For practical applications there are used only magnetic fields smaller than the exchange biased field H_{exch} for which only the magnetization from the free layer will be reversed, Fig. 5a.

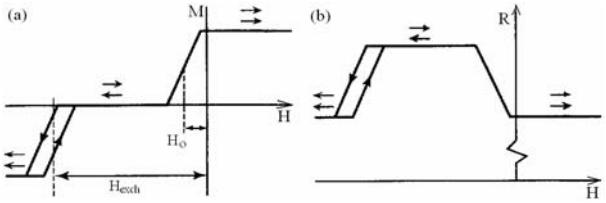

Fig. 5. Representation of (a) the magnetization curve and (b) the field dependence of the resistance of an exchange-biased spin valve. Magnetization reversal of the sensitive and the exchange-biased layer takes place at the offset field H_o and the exchange-biased field H_{exch}, respectively.

The offset field is due to the small ferromagnetic coupling between the ferromagnetic layers because of their irregular surfaces. This field is well described by the Néel model for positive magnetostatic interlayer coupling (orange peel coupling) [7]. The MR ratio $\Delta R_{GMR}/R_0$ for these exchange-biased spin valves is typically 4.5 – 6 % at room temperature. The spin valves also show a small AMR effect, with a MR ratio of about 1 % or less.

GMR devices are typically operated with the sense current in the plane of the films (CIP, current-in-plane) using electrical contacts at the ends of long, often serpentine, lines. Although the magnetoresistance is reduced because of current shunting through the layers the alternative current-perpendicular-to-pane (CPP) configuration will typically have a resistance that is too low for practical circuit applications. However, by combining the semiconductor structures with magnetic thin films technology, a new type of magnetic field sensor named the *spin-valve transistor* [8] was developed. The spin-valve transistor consists of a silicon emitter, a CPP Co/Cu magnetic multilayer as the base and a silicon collector. Electrons are injected from the emitter, passing the first Schottky barrier (semiconductor-metal interface) into the base. Because of the thin base multilayer (10 nm), most of the electrons are not directed to the base contact, but travel perpendicular through the multi-layer across the second Schottky barrier. These electrons form the collector current. The number of electrons that reach the collector increases exponentially with the mean free path of the electrons in the base. But the mean free path varies with the applied magnetic field, hence the collector current becomes strongly magnetic field dependent.

Tunneling Magnetoresistance (TMR) structures are similar to CPP spin valves except that they utilize an ultra-thin insulating layer to separate two magnetic layers rather than a conductor. Electrons pass from one layer to the other through the insulator by quantum mechanical tunneling. The ease of tunneling between the two magnetic layers is modulated by the angle between the magnetization vectors in the two layers. When the magnetization of the layers is aligned many states are available in the bottom layer for spin-polarized electrons from the top layer to tunnel into. When the magnetization directions are opposite, the spin polarized electrons are prevented from tunneling because they have the wrong orientation to enter the bottom layer. The process is also known as spin-dependent tunneling (SDT). The SDT effect is used for building high sensitivity magnetic sensors, read head for high density data storage devices and nonvolatile magnetic memories (MRAM).

2. Results and discussion

2.1. Micromagnetic characterization of a rotation sensor based on the anisotropic magnetoresistance effect

We used three samples to study the angular dependence of the AMR effect: (i) a $Ni_{80}Fe_{20}$(10 nm) film, (ii) a $Ni_{80}Fe_{20}$(10 nm)/Cu(4 nm)/$Ni_{80}Fe_{20}$(10 nm) multilayer structure and (iii) a $Ni_{80}Fe_{20}$(2 nm)/Al_2O_3(1 nm)/$Ni_{80}Fe_{20}$(2 nm) nanogranular film. The multilayer structure presents, in addition to the AMR effect, a small GMR effect. Details regarding the samples preparation were given in a previous work [9]. The four-lead setup used to investigate the angular dependence of the PHE is presented in Fig. 6(a). The equivalent resistor arrangement model [3] is presented in Fig. 6(b) and helps us to understand the angular behaviour of the PHE voltage. Also it is shown the orientation of the magnetic field vector which is applied in the film plane. The DC current sources I_1 and I_2 drive the same current, I, through the sample, S, and are computer controlled. When the source I_1 is ON, the source I_2 is OFF and the measured PHE voltage is U_1.

When the source I_2 is ON, the source I_1 is OFF and the measured PHE voltage is U_2. In this way, for a given angle, θ, between the magnetic field, H, and the direction of the current driven by I_1, we made two measurements for the PHE. Because for an ideal experimental setup U_1=U_2 we will take as reference for angle measurements the direction of the current I_1 for both measurements.

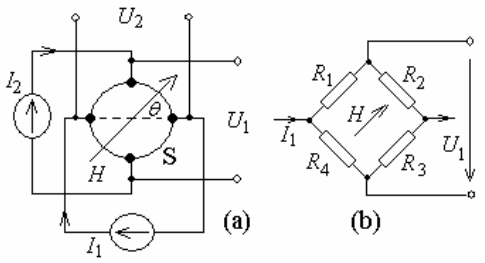

Fig. 6. (a) Schematic setup used for PHE measurements and (b) the four-resistor arrangement model to account for the electric behaviour of the sample. H is applied in the sample plane.

The PHE voltage was detected by a 2 channel Keithley digital voltmeter 2182A with a precision better than 100 nV. The angular dependence was achieved by using a stepper-motor allowing rotation with a precision of 0.1° and the results of the measurements made on these samples, voltage U_1, are presented in Fig. 7.

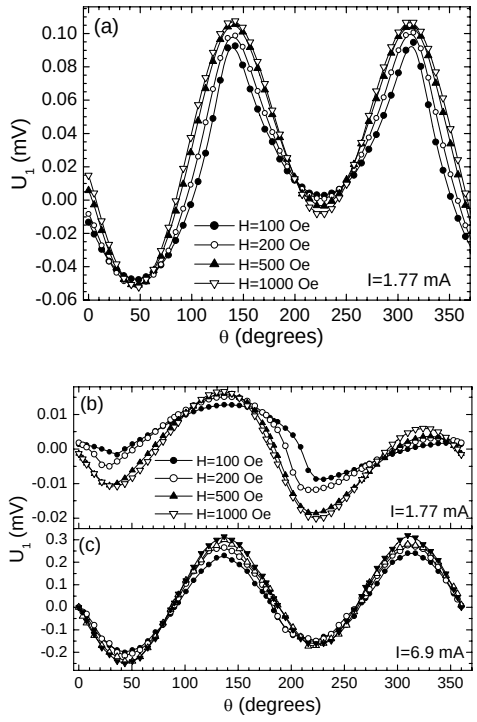

Fig. 7. Angular dependencies of the PHE effect, for different values of the applied field, measured for (a) $Ni_{80}Fe_{20}$(10 nm) film, (b) $Ni_{80}Fe_{20}$(10 nm)/Cu(4 nm)/$Ni_{80}Fe_{20}$(10 nm) ML and (c) $Ni_{80}Fe_{20}$(2 nm)/Al_2O_3(1 nm)/$Ni_{80}Fe_{20}$(2 nm) nanogranular film.

Because of the contacts misalignments the angular behaviour of the PHE, voltage U_1, is distorted. For magnetic fields lower than 200 Oe the PHE voltage depends also on the amplitude of the applied field because the magnetization is less than the saturated value. On the other hand, we see that for the ML sample, Fig. 7(b), the angular dependencies of the PHE voltage for low magnetic fields (H=100 and 200 Oe respectively) present some irregularities that are far from the shape predicted by the eq. 2. This is because the magnetization cannot follow accurately the direction of the magnetic field due to the coupling effects between the magnetic layers through the Cu layer. Despite of the good response of the $Ni_{80}Fe_{20}$(2 nm)/Al_2O_3/$Ni_{80}Fe_{20}$(2 nm) nanogranular film, Fig. 7(c), the thermal stability is not good because of the conduction mechanism through the oxide barriers which give a negative thermal coefficient of the resistivity.

To understand the behaviour of the PHE at low magnetic fields for $Ni_{80}Fe_{20}$(10 nm) thin film and $Ni_{80}Fe_{20}$(10 nm)/Cu(4 nm)/$Ni_{80}Fe_{20}$(10 nm) multilayer structure, we performed micromagnetic simulations, based on Stoner-Wolfarth theory, to obtain the angular dependence of the sample magnetization for different values of the rotating magnetic field. To make these simulations, we used a complex structure of single domains of Permalloy which interact between them and with the applied magnetic field [9,10]. We can see in Fig. 8(a) the results of the micromagnetic simulations for angular dependence of the magnetization for $Ni_{80}Fe_{20}$(10 nm) thin film and for the ML structure in Fig. 8c.. To run these simulations we assumed the samples saturated and then the magnetic field was rotated from 0 to 720° counter clockwise and then back to 0. In this way we were able to put in evidence hysteretic behaviour of the angular dependence of magnetization for low magnetic fields. As we can see, for magnetic fields higher than 200 Oe, the angular dependence of the film magnetization tends to become a line. This means that the sample's magnetization will have a constant value and his orientation follows the orientation of the applied magnetic field.

Using the results of these micromagnetic simulations we were able to calculate the angular dependencies of the PHE which are presented in Fig. 8b and Fig. 8d.. For magnetic fields higher than 200 Oe the sample saturates and the PHE voltage will depends only on the rotation angle, θ. This is important from practical point of view because the sensor response will be immune to small fluctuations of the applied magnetic field. We can observe, for the ML structure, strong fluctuations of the magnetization and hysteretic effects when the magnetic field is lower than 200 Oe. The PHE response presents some irregularities that are far from the shape predicted by the eq. 2. These results are in good agreement with the PHE measurements presented in Fig. 7(b).

To compensate the errors due to contacts misalignment and to increase the sensor sensitivity we made two measurements of the PHE voltage for each angle over two orthogonal directions using the setup presented in Fig. 6(a). Making the PHE measurements for Permalloy and the ML structure over these two orthogonal

directions we obtained, by summating the voltages U_1 and U_2, a response of the sensor which is well described by the eq. 2. The results of these measurements made on $Ni_{80}Fe_{20}$(10 nm) and $Ni_{80}Fe_{20}$(10 nm)/Cu(4 nm)/$Ni_{80}Fe_{20}$(10 nm) thin films were reported in [9]. The calculated values $U_S=U_1+U_2$ give us the output of the rotation sensor with a sinusoidal behaviour with two periods for a complete rotation.

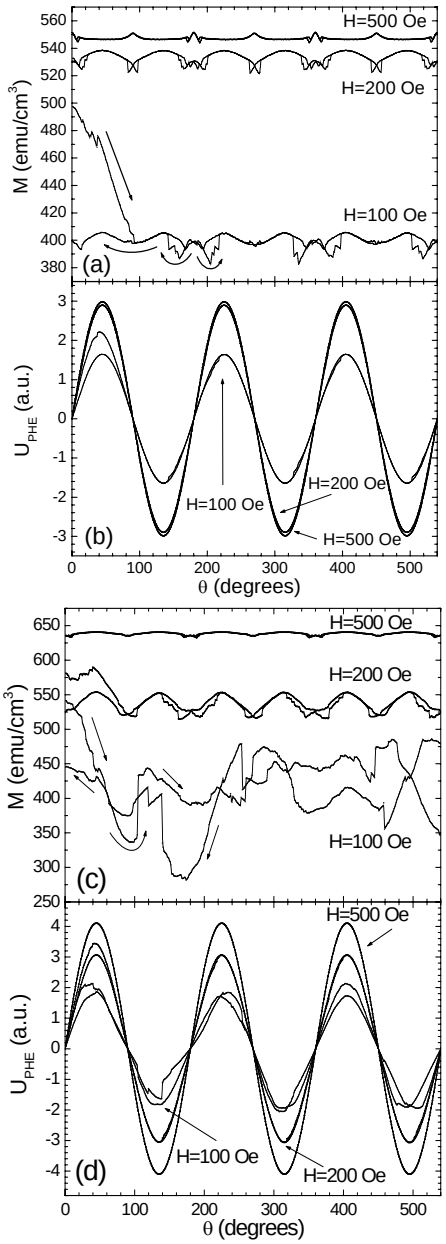

Fig. 8. (a) Micromagnetic simulations for the angular dependence of the magnetization and (b) the calculated PHE response for different values of the applied magnetic field for $Ni_{80}Fe_{20}$(10 nm) thin film. (c) Micromagnetic simulations for the angular dependence of the magnetization and (d) the calculated PHE response for the $Ni_{80}Fe_{20}$(10 nm)/Cu(4 nm)/$Ni_{80}Fe_{20}$(10 nm) ML structure.

2.2 Detection of magnetic particles used in biological applications

In this subsection we describe the detection of magnetic beads labeled with different biological structures. Magnetic micro-beads when magnetized by an external field have a magnetic dipole field as we sketched in Fig. 9a. This field is proportional to the volume of magnetic material and inversely proportional to the distance cubed. So, detecting these small fields is increasingly difficult as the distance from the bead to the sensor increases. On the other hand, if the sensitive area is much larger than the bead, only the portion of the magnetoresistive material close to the bead will be affected. Therefore the fractional change in resistance, and hence the sensitivity, will be maximized by matching, if is possible, the size of the sensor to the size of the bead and by reducing the distance between the sensor and the bead. This requirement matches the attributes of GMR sensors. The amplitude of stray fields produced by the beads depends on the nature and particle dimension. In our simulations regarding the sensor response we'll assume a total thickness of the layers (immobilization layer and protection layer – Si_3N_4) between the bead and the GMR sensor of 0.2 μm. The sensor dimensions are 1x1x0.1μm^3. The bead is assumed to be a sphere with a diameter of about 0.5 μm. The saturation magnetization of the micro-magnetic bead is 400 emu/cm^3. For an external magnetic field of 500 Oe, the amplitude of the stray field in the sensor region, under the above conditions, is between 8 and 24 Oe.

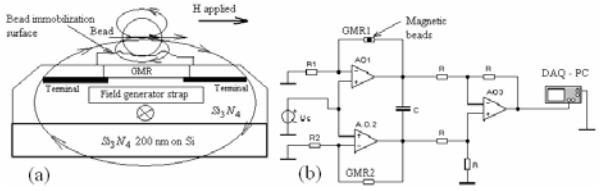

Fig. 9. (a) The schematic setup for a GMR sensor that detects the stray field generated by a bead and (b) the differential measurement setup used to measure the stray field produced by the magnetic bead. The sensor GMR2 is used as reference.

In order to extract the contribution corresponding to the total magnetic moment of the bead and to avoid the influence of the external magnetic fields and thermal variations we designed a differential measurement system like in Fig. 9b. From basic electronics, we have for the output voltage that is applied to the data acquisition system the expression (in modulus):

$$\Delta U = \left(U_{GMR1} + U_C\right) - \left(U_{GMR2} + U_C\right) = U_{GMR1} - U_{GMR2} = f\left(H_{bead}\right) \tag{4}$$

where H_{bead} denotes the strength of the stray field generated by the magnetic bead in the sensor region.

The micromagnetic simulations for a differential measurement system, according to physical and electronic

setup shown in Fig. 9, are presented in Fig. 10(a) when the magnetic field is applied parallel to the easy axis and in Fig. 10(b) when the magnetic field is applied perpendicular to the easy axis. The results show only the contribution of the stray fields produced by the micro-bead. The output, ΔU, of the differential amplifier is directly proportional to the changes of the GMR amplitude that takes place in the sensor GMR1 due to the presence of the micro-bead at 200 nm above.

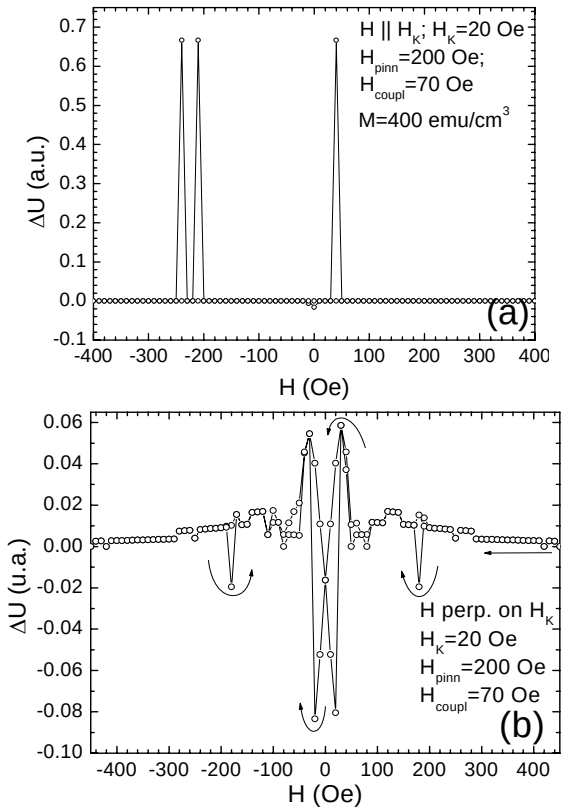

Fig. 10. The response of a differential system with GMR sensors for a magnetic micro-bead placed 200 nm above the sensor GMR1, when the magnetic field is applied (a) parallel and (b) perpendicular to the easy axis. The GMR sensors consist of multilayer structures as FeMn/NiFe(2 nm)/Cu(1 nm)/NiFe(2 nm) for which we assumed a small positive coupling between the magnetic layers through the nonmagnetic layer, H_{coupl}=70 Oe and a uniaxial anisotropy field H_K=20 Oe.The arrows are guide for the eyes.

3. Conclusions

In this paper we presented, using a phenomenological approach, an overview of the magnetoresistive effects (AMR, GMR and TMR) that are used to build sensors made from magnetic layers and nanostructured systems. The spin valve mechanism was presented. Finally, we presented a micromagnetic characterization and a method to increase the response quality of a rotation sensor based on the anisotropic magnetoresistance effect. A detection system of the magnetic particles employed in biology as markers or as carriers for targeted drug delivery was presented as well.

References

[1] J. C. S. Kools, R. Coehoorn, W. Folkerts, M. C. De Nooijer, G. H. K. Somers, Philips J. Research **51**, 125 (1998).
[2] L. Balcells, E. Calvao, J. Fontcuberta, J. Magn. Magn. Mater. **242-245**, 1166 (2002).
[3] C. Prados, D. Garcia, F. Lesmes, J. J. Freijo, and A. Hernando, Appl. Phys. Lett. **67**, 718 (1995).
[4] F. Montaigne, A. Schuhl, F. Nguyen Van Dau, A. Encinas, Sensors and Actuators **81**, 324 (2000).
[5] M. Volmer, J. Neamtu, J. Optoelectron. Adv. Mater. **5**(4), 951 2003.
[6] E. M. Epshtein, A. I. Krikunov, Yu. F. Ogrin, J. Magn. Magn. Mater. **258-259**, 80 (2003).
[7] J. C. S. Kools, Th. G. S. M. Rijks, A. E. M. De Veirman, R. Coehoorn, IEEE Trans. Magn. **31**, 3918 (1995).
[8] D. J. Monsma, J. C. Lodder, Th. J. A. Popma, B. Dieny, Physical Review Letters **74**, 5260 (1995).
[9] M. Volmer, J. Neamtu, J. Magn. Magn. Mater, **316,** e265 (2007).
[10] M. Volmer, J. Neamtu, Physica B **372**, 198 (2006).

*Corresponding author: volmerm@unitbv.ro